From Points to Lines to Surfaces: A Novel Approach to Reconstructing Field-Scale Three-Dimensional Shale Roof Models Using Image Processing

Gaobo Zhao, Deniz Tuncay
Department of Mining Engineering, West Virginia University

Mindi Ruan
Lane Department of Computer Science and Electrical Engineering, West Virginia University

Ihsan Berk Tulu, Yuting Xue
CDC NIOSH, Pittsburgh Mining Research Division

Xin Li
Department of Computer Science, University at Albany, SUNY

ABSTRACT

Most coal mine roofs in the Appalachian region consist of laminated shale, which is prone to brittle failure. Accurate modeling of shale roofs is vital for studying cutter failures of these shale roofs, and ordinary and formational bedding planes play a significant role in the response of the shale roof to mining-induced stresses. This paper presents a robust method for constructing three-dimensional shale roof models using limited borehole cores and leveraging image processing techniques. The approach begins with image extraction from shale cores. Then, we extract the portions that feature the core and employ image-stitching techniques to merge them seamlessly. Once the images are stitched, they are duplicated horizontally and merged to create a cross-sectional plane image representing a shale roof. This roof cross-sectional plane image serves as an input to our proprietary Digital Image Processing (DIP) algorithm, which is adept at extracting ordinary bedding planes (interfaces that represent color transitions between a single shale unit). The extraction process involves transforming discrete core points (ordinary bedding plane pixels) into continuous lines representing ordinary bedding planes. Finally, extending this method into the third dimension, the model is further extrapolated to form a comprehensive three-dimensional shale roof. Through this process, the geometry information of ordinary bedding planes can be extracted for each type of shale in cores, including sandy shale, gray shale, dark shale, etc. This work bridges the gap between limited core data and comprehensive 3D geological modeling, offering valuable insights into identifying and quantifying the variations in different shale roof geologies.

INTRODUCTION

In the United States, underground coal mines are primarily located in the Appalachian region, the Interior region, and the Western region. Among these regions, the Appalachian region has consistently supplied more than half of the underground coal production, accounting for approximately 58% over the past decade, totaling around 16 million short tons per year (EIA—US Energy Information 2022). Nevertheless, underground coal mines in this region face a potential risk of roof collapses due to thinly laminated weak shale roof geologies, especially in West Virginia, Pennsylvania, and Kentucky (Bajpayee et al. 2014; Zhao et al. 2022). Most coal mine roofs in this region consist of laminated shale, which is prone to brittle failure and may collapse after mining excavations, as shown in Figure 1.

According to Figure 1, a shale roof consists of one or several units of shale lithology, including gray shale, sandy shale, dark shale, etc. The interface between each unit can be captured through the Mine Roof Geology Information System (MRGIS) developed by Peng (2005). The locations of these interfaces are of particular interest to mining engineers. Each shale unit's thickness ranges from 0.2 to 5 m, which encompasses ordinary bedding planes (interfaces that represent color transitions between a single shale unit) that contribute to the details of shale roof geological features. However, previous studies often oversimplified ordinary bedding planes, assuming them to be continuous, straight, and equidistant. This oversimplification falls short of addressing the diverse and complex variations found in shale roofs. Modifications or even complete redesigns of existing support technologies become necessary to accommodate these variations, as changes in ordinary bedding planes significantly impact shale behavior, potentially leading to support system failure. Thus, the primary challenge lies in dealing with the oversimplified ordinary bedding planes in shale roofs.

Detection of ordinary bedding planes is challenging due to their complex nature (Li et al. 2022). Machine learning methods for

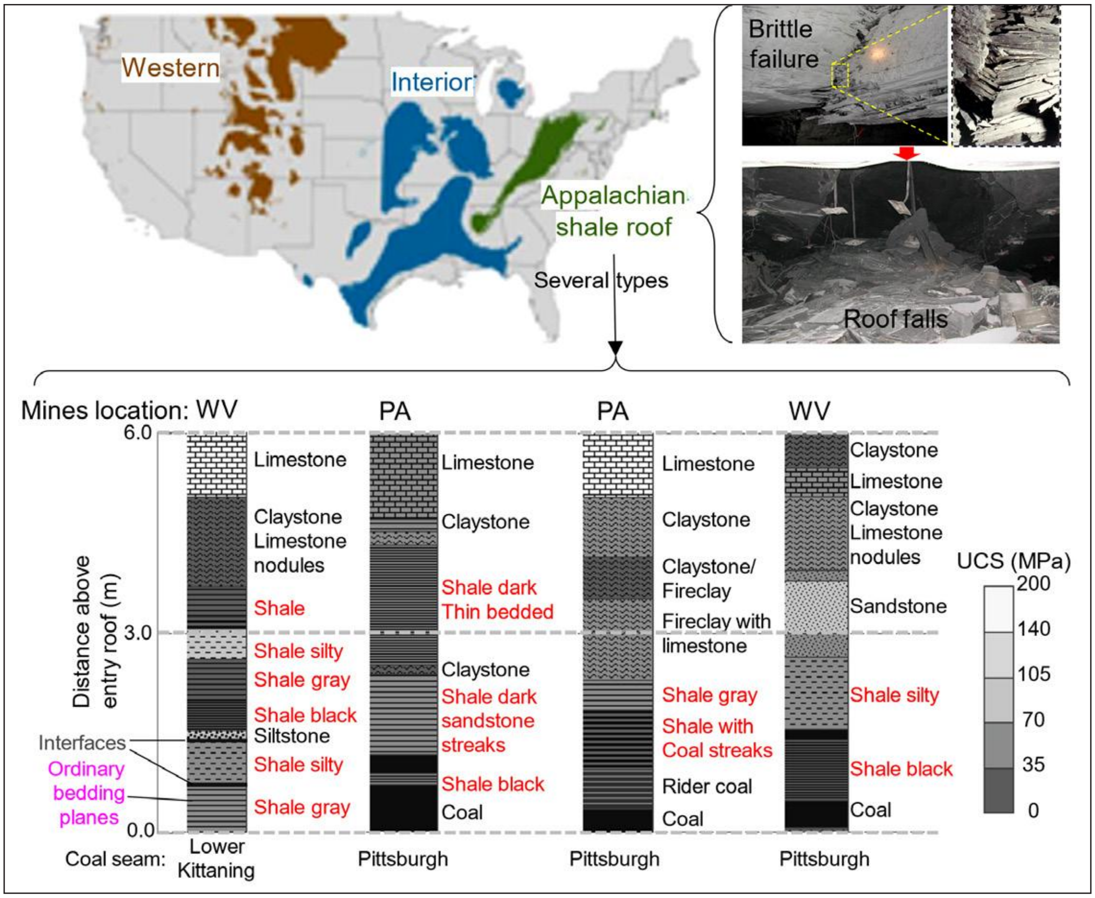

Figure 1. Shale roofs in the Appalachian region, interfaces between each distinct lithology, and ordinary bedding planes (after Esterhuizen et al. 2021)

identifying ordinary bedding planes introduce challenges stemming from data quality, distribution intricacies, and the dense arrangement of bedding planes. These approaches typically demand substantial volumes of high-quality training data and involve tuning numerous parameters in the model's architecture. Similarly, point-cloud methods also confront limitations when applied to detecting ordinary bedding planes in underground coal mines. These limitations encompass issues related to resolution, accuracy, noise reduction, the presence of artifacts, consideration of surface properties, and computational requirements.

In this paper, based on the work of Zhao et al. (2023), a novel approach to reconstructing field-scale 2D/3D shale roof models was developed based on a Digital Image Processing (DIP) algorithm, which is adept at extracting ordinary bedding planes in shale roofs from cores. The geometry information of ordinary bedding planes can be extracted for each unit of shale in cores, including sandy shale, gray shale, dark shale, etc. This method enables more accurate and efficient detection of ordinary bedding planes compared to manual annotation, providing reliable data for subsequent numerical modeling on shale roofs.

METHODOLOGY

2.1 Image Formation of Shale Roof Cross-Section

In our image extraction methodology, we take images from three types of shale long core, as shown in Figure 2. According to Figure 2b, gray shale has the most diverse range of broken segment lengths, and black shale has comparatively shorter lengths. This indicates that the black shale is weaker than others since it is more prone to breaking during coring.

The shale core is divided into three sections. Each section is photographed, as illustrated in Figure 3. We ensure that adjacent sections have a suitable overlap, which significantly enhances the performance of the subsequent image-stitching process. This image-stitching technique, i.e., AutoStitch, is specifically employed to address the issue of straight bedding planes in the long core appearing as curved lines in the captured images (Brown and Lowe 2007). By carefully aligning and merging the overlapping images, we effectively rectify this distortion, ensuring that the linear features of the bedding planes are accurately represented in the final composite image. Then, the pixel size of each type of shale can be calculated by dividing the image length by the number of pixels along the image length.

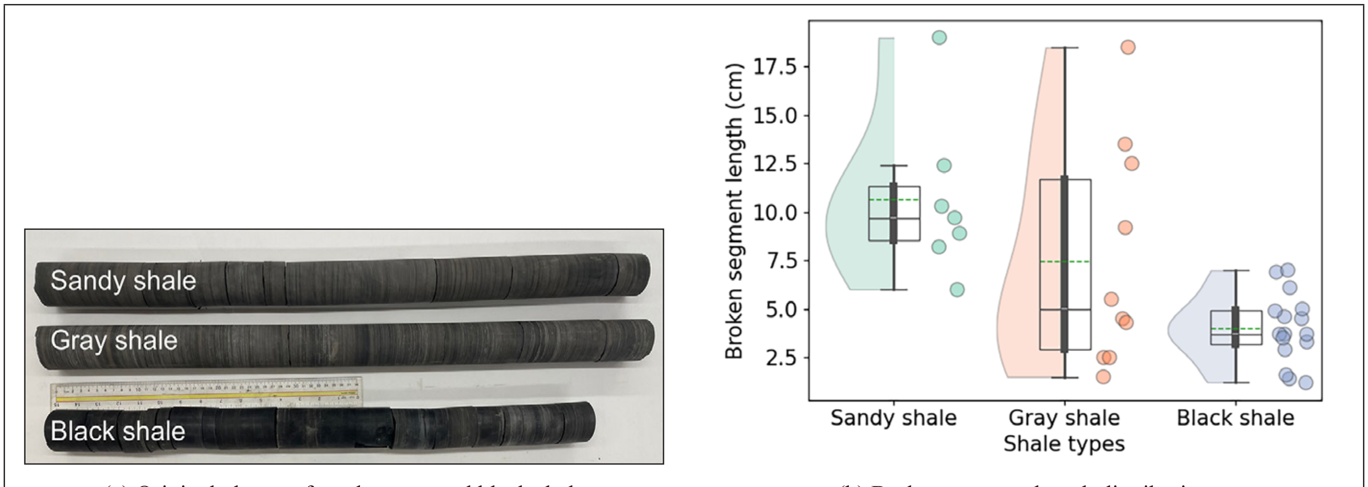

(a) Original photos of sandy, gray, and black shale
(b) Broken segment length distribution

Figure 2. Three types of shale long core photo and core sample length distribution

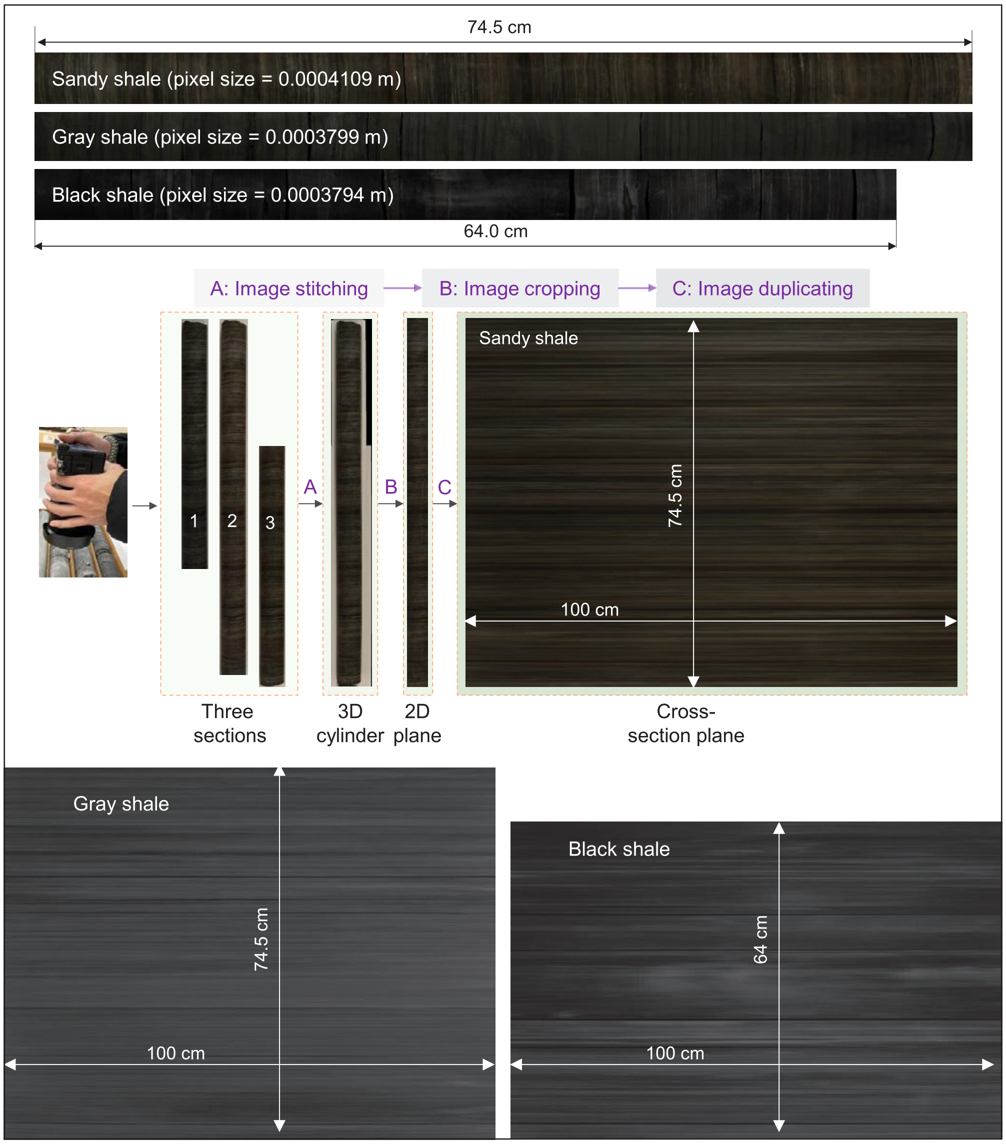

Figure 3. Image formation process of shale roof cross-section plane

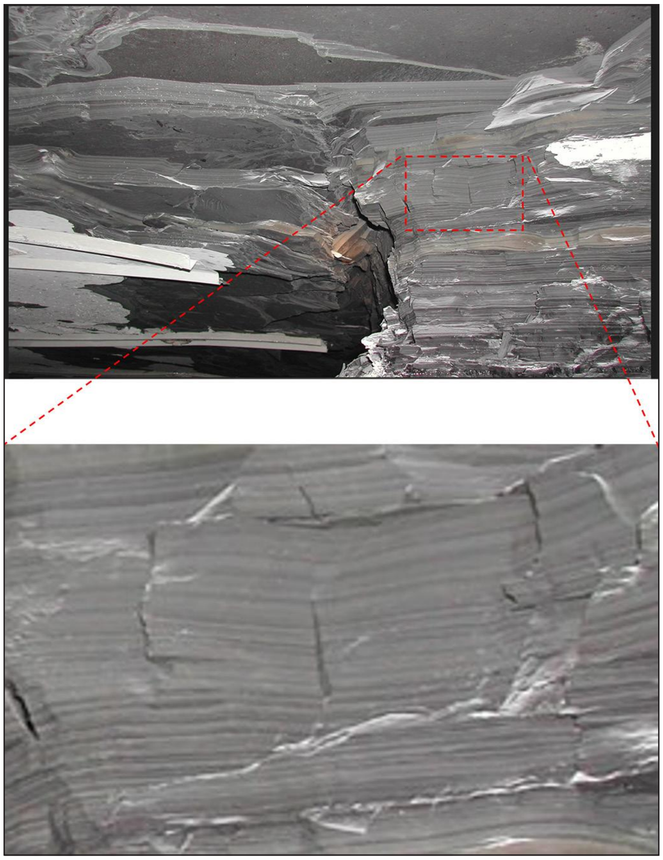

Figure 4. Exposed shale roof cross-section with continuous ordinary bedding planes observed in the field

Following the image stitching, we focus on cropping the regions of the images that are of particular interest. These cropped images are then duplicated and further merged to create a cross-sectional representation of a partial shale roof, measuring 100 cm in width and 74.5 cm in height for sandy shale and gray shale, and 100 cm in width and 64 cm in height for black shale, as shown in Figure 3.

These processes would be applied to various types, including sandy shale, gray shale, and black shale. These composite images accurately portray continuous ordinary bedding planes, closely resembling those seen in the exposed cross-section of the shale roof within a stable geological setting, as demonstrated in Figure 4. This image thus serves as an effective surrogate, allowing us to deduce the structure of the shale roof by examining the bedding planes present in the core.

2.2 Point: Ordinary Bedding Plane Pixel Detection

Shale is distinguished from other rocks by its laminated and fissile nature, as it consists of many thin layers and easily splits into thin pieces along the ordinary bedding planes (Speight 2013). Each ordinary bedding plane indicates a change in sediment deposition conditions. Taking advantage of this physical property, we used the Canny edge detector to capture the ordinary bedding plane boundaries that are combined from the ordinary bedding plane pixels (Canny 1986).

The process of edge detection can be divided into four steps:

1. Noise reduction: After taking images from shale cores, the images are smoothed using a Gaussian filter to mitigate the effects of noticeable noise.
2. Gradient calculation: After noise reduction, Sobel filters are applied to the image to calculate the gradient in each pixel of the image that indicates the direction and intensity of the sharpest change in intensity.
3. No-maximum suppression: Based on the calculated gradient intensity of each pixel, the algorithm goes through all the pixels on the gradient intensity. If a pixel's gradient intensity is not the maximum among the pixels in its edge direction, it will be suppressed to zero. The purpose of this step is to thin the edges at one-pixel size.
4. Double thresholding: Due to the nature of previous work (Zhao et al. 2023) being focused on lab-scale studies, attention was given to interim bedding planes with a layer thinner than 1 cm, i.e., lamina (McKee and Weir 1953). For this purpose, interval thresholding was employed. In contrast, this study targets larger-scale shale formations and is primarily concerned with the most macroscopically significant bedding planes, i.e., ordinary bedding planes. Consequently, we have adopted the original double thresholding technique of the Canny Edge Detection algorithm (Canny 1986) for our analysis. The Canny algorithm utilizes two thresholds—a high and a low (i^{low} and i^{high})—to effectively differentiate between strong, weak, and non-relevant edges. Strong edges are those exceeding the high threshold, while weak edges, situated between the high and low thresholds, are either retained or discarded based on their connectivity to strong edges. Specifically, a weak edge is preserved if it is directly connected to a strong edge or forms part of a continuous chain of weak edges leading to a strong edge. This methodology is particularly suited for our study, as it allows for a more focused and precise identification of the most prominent bedding planes in larger-scale shale formations.

Based on the above four steps, the ordinary bedding plane pixels can be detected, which is presented in Section 3. It is important to note that the output of the above four steps does not provide precise information on the specific set of points defining a given ordinary bedding plane. It only determines whether a pixel belongs to an ordinary bedding plane. Therefore, the next step is to connect points or disconnected ordinary bedding planes to lines, presenting 2D ordinary bedding planes.

2.3 Line:2D Ordinary Bedding Planes Representation

Similar to Zhao et al. (2023), a depth-first search (DFS) algorithm is introduced to group pixels belonging to the same ordinary bedding plane. The difference from Zhao et al. (2023) is the size of the search window. Here, in the field scale, we use a larger size, which is with a height of 5 pixels and a base of 6 pixels, placing the currently traversing ordinary bedding plane pixel at its top center. The dimensions of these search windows can be adjusted depending on the image size, typically maintaining a height-to-base ratio of 5:6.

Subsequently, the algorithm traverses each ungrouped ordinary bedding plane pixel within this search window. If it identifies additional ordinary bedding plane pixels associated with ordinary bedding planes, it classifies them as belonging to the same plane as the currently traversing ordinary bedding plane pixel. This cycle repeats until all ordinary bedding plane pixels from the same ordinary bedding plane are clustered into a cohesive group.

Upon completion of the ordinary bedding plane pixel clustering, we implement a threshold to the results. Represented as "*n*," the threshold corresponds to the number of points/pixels in an ordinary bedding plane. It allows us to disregard any plane with fewer than "*n*" points, interpreting them as noise. The image lengths of sandy shale, gray shale, and black shale are 2,277, 2,346, and 2,093 pixels, respectively. In this paper, we set $n = 2000$, which means that the ordinary bedding plane will be continuous almost throughout the whole image length, which matches well with the field observations.

After that, to facilitate the application in UDEC (Itasca 2023a), we implement a point simplification process to extract representative points for the coordinates of the ordinary bedding planes. Our approach capitalizes on three key points to portray an ordinary bedding plane, enhancing its applicability in UDEC. These three representative points encompass the two endpoints of the line segment and a middle point, computed as the average of all point coordinates. The results are shown in Section 3.

This approach of utilizing representative points offers an efficient and flexible method to capture the essential characteristics of bedding planes. Moreover, the middle point can serve as an offset for errors introduced by the DFS algorithm.

2.4 SURFACE: 3D ORDINARY BEDDING PLANES

After obtaining the 2D coordinates of ordinary bedding planes, to facilitate the application in 3DEC (Itasca 2023b) for generating a 3D shale roof model, we extend each 2D line to a surface by adding one more axis for each ordinary bedding plane. This transformation is carried out by adding a y-coordinate to each point on the line. The y-coordinate is introduced with values ranging from 0 m at the lower end to 1 m at the upper end, effectively creating a surface that spans the height of the y-axis. The upper end can be modified according to the specific shale roof conditions. The results are shown in Section 3.

RESULTS

3.1 i^{low} and i^{high} Selection

As discussed in Section 2.2, the double thresholds of i^{low} and i^{high} have a significant influence on the detection of the ordinary bedding plane pixels. Selecting an optimum i^{low} and i^{high} is vital to the final results. Taking sandy shale as an example, the ordinary bedding plane pixel detection results with different values of i^{low} and i^{high} are shown in Figure 5.

From Figure 5a, when i^{low} is fixed at 0, it is obvious that the number of detected ordinary bedding plane pixels decreases as i^{high} increases. A higher i^{high} corresponds to detected pixels representing a greater gradient intensity. This indicates the presence of a strong, contrasting color or texture that stands out from the surrounding sediment. Conversely, with a lower i^{high}, not only pixels with

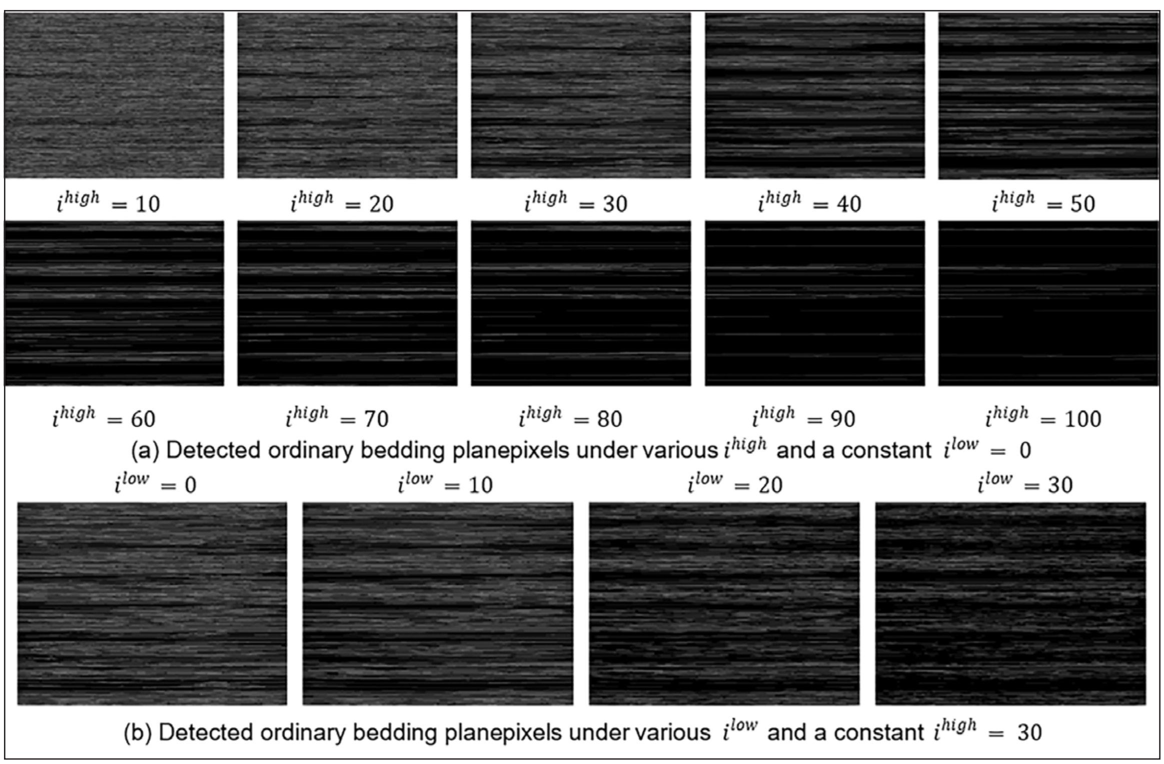

Figure 5. Effects of i^{high} and i^{low} on ordinary bedding plane pixel detection results in sandy shale

Table 1. Beds number of each type of shale under different i^{high} (i^{low} = 0 here)

Sandy shale						
i^{high}	30	40	50	60	70	80
Laminas number	62	56	37	23	9	7
Beds number	24	23	26	28	24	17
Percentage of beds	27.91%	29.11%	41.27%	54.90%	72.73%	70.83%
Percentage of losing beds	0.00%	4.17%	–8.33%	–16.67%	**0.00%**	29.17%
Gray shale						
i^{high}	30	40	50	60	70	80
Laminas number	17	8	4	2	1	1
Beds number	31	22	10	7	6	6
Percentage of beds	64.58%	73.33%	71.43%	77.78%	85.71%	85.71%
Percentage of losing beds	**0.00%**	29.03%	67.74%	77.42%	80.65%	80.65%
Black shale						
i^{high}	30	40	50	60	70	80
Laminas number	19	15	12	11	7	4
Beds number	28	25	25	21	16	11
Percentage of beds	59.57%	62.50%	67.57%	65.63%	69.57%	73.33%
Percentage of losing beds	0.00%	10.71%	**10.71%**	25.00%	42.86%	60.71%

Note: Laminas are the layers with thickness less than 1 cm, while beds are the layers with thickness 1~5 cm.

higher gradient intensity are detected but also those with lower gradient intensity. When i^{high} is too low (10 and 20), noise becomes detectable.

From Figure 5b, when i^{high} is fixed at 30, the number of detected ordinary bedding plane pixels slightly decreases as the i^{low} increases. In comparison to i^{low}, i^{high} has a more substantial impact on the detection of ordinary bedding plane pixels. Subsequently, fixing i^{low} at 0, we proceed to select the optimum i^{high}.

In shale, each layer among these distinct layers is termed a bed, representing the fundamental unit of stratigraphy. Technically, a bed is defined as a bedding plane thicker than 1 cm. A layer thinner than 1 cm is referred to as a lamina (McKee and Weir 1953). In this paper, we focus on detecting beds at the field scale, i.e., layers thicker than 1 cm. We assume that the number of thick layers (>1 cm) we obtain from i^{high} = 30 is the maximum and aim to retain 90% of those. In other words, we should not lose more than 10% of them and should aim to eliminate the thin layers. Based on this idea, we summarized the bed count for each type of shale under different i^{high} values, as shown in Table 1.

From Table 1, we observed that for sandy shale, i^{high} = 70 resulted in a 0.00% loss of beds; for gray shale, i^{high} = 30 led to no loss of beds; and for sandy shale, i^{high} = 50 resulted in a 10.71% loss of beds. If the i^{high} exceeds these values, it results in losing more beds. Therefore, we select i^{high} = 70 for sandy shale, i^{high} = 30 for gray shale, i^{high} = 50 for black shale.

3.2 2D Ordinary Bedding Plane Detection Results

According to the above-determined i^{low} and i^{high} of each type of shale, the results of pixel detection, pixel cluster by DFS, and 2D ordinary bedding plane representation are shown in Figure 6. The corresponding ordinary bedding plane spacing distribution is shown in Figure 7.

From Figure 7, it is observed that most of the spacings exceed 1 cm. The average spacings of ordinary bedding planes in sandy shale, gray shale, and black shale are 2.40 cm, 1.51 cm, and 1.83 cm, respectively. Notably, black shale exhibits the most diverse range of spacing, while sandy shale and gray shale display a less diverse range. This suggests that sandy shale and gray shale present a regular texture indicative of sedimentary material changes, whereas black shale does not.

3.3 2D/3D Modeling on Ordinary Bedding Planes

After detecting 2D ordinary bedding planes, the coordinates of three representative points, encompassing the two endpoints of the line segment and a middle point, are imported into UDEC using the commands 'DFN,' 'fracture import,' and 'geometry edge create by-position.' The results are shown in Figure 8 (left). Furthermore, we add a y-coordinate to each point on the line to create a surface in 3DEC that spans the height of the y-axis, using the commands 'DFN,' 'fracture import,' and 'geometry polygon create by-position.' The results are shown in Figure 8 (right). The obtained 2D/3D modeling of ordinary bedding planes of sandy shale, gray shale, and black shale provides an important basis for further analysis of roof deformation and roof support design.

It is important to note that the three types of shale roof cores discussed in this paper are from an underground coal mine that excavates Pittsburgh coal seam in the Northern Appalachian coal region. The method presented above can also be used to reconstruct other types of shale cores from this or other regions. In addition, the core

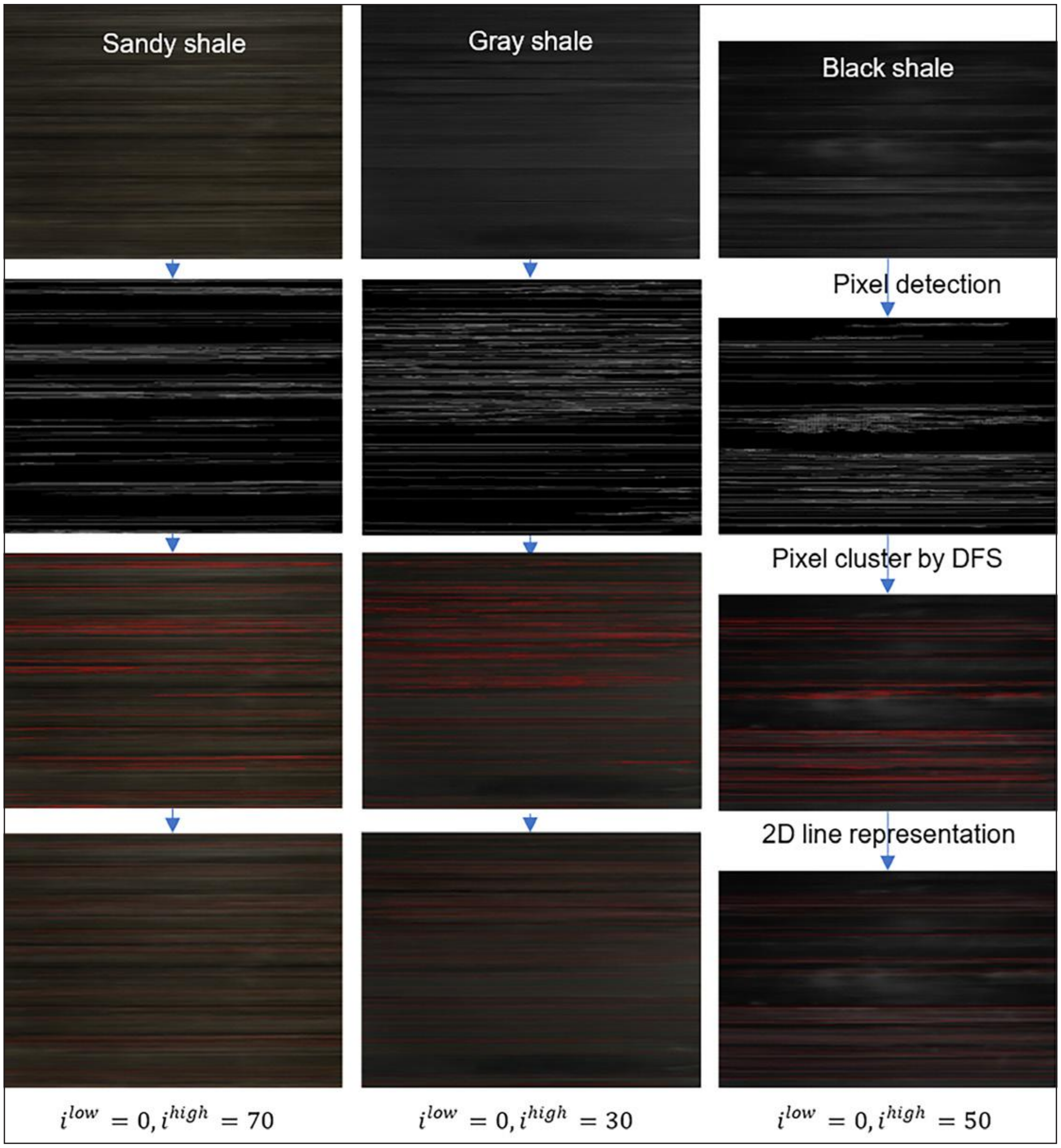

Figure 6. 2D Ordinary bedding plane in sandy shale, gray shale, and black shale

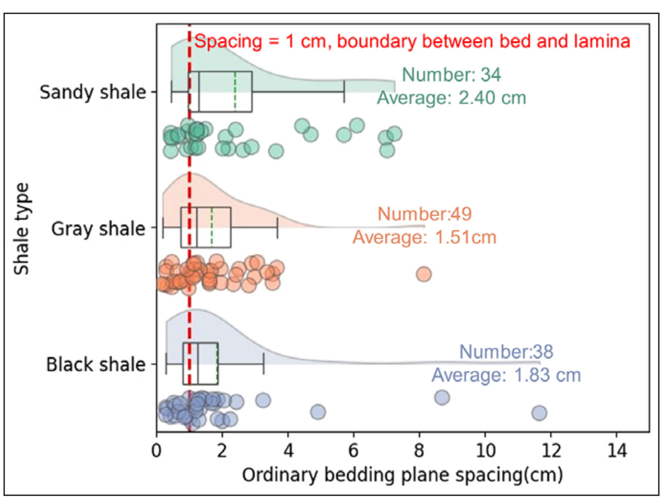

Figure 7. 2D Ordinary bedding plane spacing distribution

image can be obtained by phone, camera, and high-technology devices like infrared ray detection, X-ray computed tomography, or CT scans. In this paper, the images are captured from SONY Alpha 7C with a Sony FE 40 mm F2.5 G lens.

CONCLUSIONS

(1) A robust method for constructing 2D/3D shale roof models was developed using limited borehole cores and image processing techniques. This method involves three steps: image formation of shale roof cross-section, ordinary bedding plane pixel detection, and 2D/3D ordinary bedding plane representation.

(2) Double thresholding of $i^{low}$and i^{high} was applied to detect ordinary bedding plane pixels. $i^{low}$and i^{high} of sandy shale, gray shale, and black shale was determined based on beds losing percentage (10%). Then, the spacing distribution of ordinary bedding planes of each type of shale core was discussed.

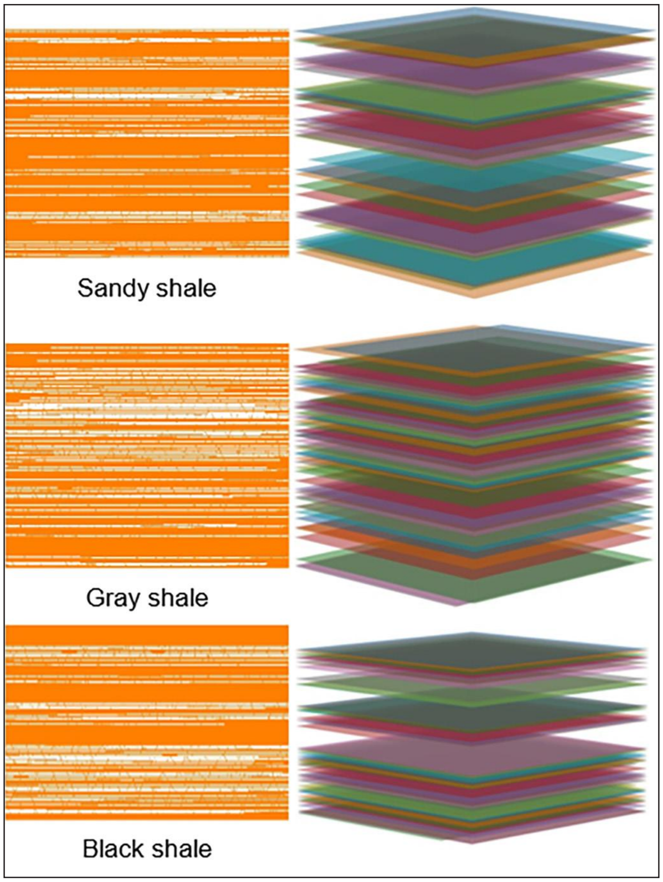

Figure 8. Ordinary bedding plane representations in UDEC (left, 2D) and 3DEC (right 3D)

(3) The obtained coordinates of ordinary bedding planes were imported into UDEC and 3DEC. The corresponding 2D/3D models of sandy shale, gray shale, and black shale were established.

LIMITATIONS OF THE STUDY

The method for constructing three-dimensional immediate roof strata models using borehole cores and image processing techniques described in this paper is still in the development stage. The findings and conclusions in this study are limited to borehole core data analyzed in this paper. The validity of the roof strata models constructed using the image processing technique described in this paper need to be verified.

ACKNOWLEDGMENTS

This work is partially supported by the WV Higher Education Policy Commission STaR Division. The authors wish to acknowledge these financial contributions and their appreciation of the organizations for supporting this basic research. The authors would like to extend their gratitude to the Alpha Foundation for the Improvement of Mine Safety Health, Inc. for funding this research study.

DISCLAIMER

This study was sponsored by the Alpha Foundation for the Improvement of Mine Safety and Health, Inc. (Alpha Foundation). The views, opinions and recommendations expressed herein are solely those of the authors and do not imply any endorsement by the Alpha Foundation, its directors, and staff.

The findings and conclusions in this report are those of the author(s) and do not necessarily represent the official position of the National Institute for Occupational Safety and Health (NIOSH), Centers for Disease Control and Prevention (CDC). Mention of any company or product does not constitute endorsement by NIOSH.

REFERENCES

Bajpayee BTS, Pappas DM, Ellenberger JL (2014). Roof instability: What reportable noninjury roof falls in underground coal mines can tell you. Prof Saf 57–62.

Brown M, Lowe DG (2007). Automatic panoramic image stitching using invariant features. Int J Comput Vis 74:59–73. https://doi.org/10.1007/s11263-006-0002-3.

Canny J (1986). A Computational Approach to Edge Detection. IEEE Trans Pattern Anal Mach Intell PAMI-8:679–698. https://doi.org/10.1109/TPAMI.1986.4767851.

EIA (US Energy Information (2022). Annual Coal Report 2021.

Esterhuizen GS, Klemetti T, Sears MM, et al. (2021). Assessing Longwall Gateroad Ground Response and Support Alternatives. Mining, Metall Explor 38:1739–1759. https://doi.org/10.1007/s42461-021-00430-x.

Itasca (2023a). UDEC 7.0 User's Guide.

Itasca (2023b). Guide to 3DEC Documentation.

Li M, Magsipoc E, Abdelaziz A, et al. (2022). Mapping Fracture Complexity of Fractured Shale in Laboratory: Three-dimensional Reconstruction From Serial-section Images. Rock Mech Rock Eng 55:2937–2948. https://doi.org/10.1007/s00603-021-02540-w.

McKee ED, Weir GW (1953). Terminology for stratification and cross-stratification in sedimentary rocks. 64:381–390.

Peng SS (2005) Evaluation of Roof Bolting Requirements Based on In-Mine Roof Bolter Drilling-Final Report. Morgantown, WV.

Speight J (2013) Shale gas production processes. Gulf Professional Publishing.

Zhao G, Ruan M, Tulu IB, et al. (2023) Reconstruct laminated shale cores/specimens for numerical modeling by physics-informed image processing. 57th US Rock Mech Symp. https://doi.org/10.56952/ARMA-2023-0732.

Zhao G, Tulu IB, Peng SS, Tuncay D (2022). Characteristics of abutment pressures and bolt loads in longwall system: A review on stress/load measurements. 41st Int Conf Gr Control Mining, ICGCM 2022 109–121.

PROCEEDINGS OF THE 43rd International Conference ON GROUND CONTROL IN MINING

ICGCM 2024

Edited by

Ted Klemetti | Rudrajit Mitra | Michael Murphy | Kyle Perry | Ihsan Berk Tulu

SME Society for Mining, Metallurgy & Exploration®

Society for Mining, Metallurgy & Exploration (SME)
12999 E. Adam Aircraft Circle
Englewood, Colorado, USA 80112
(303) 948-4200 / (800) 763-3132
www.smenet.org

The Society for Mining, Metallurgy & Exploration (SME) is a professional society whose more than 15,000 members represents all professionals serving the minerals industry in more than 100 countries. SME members include engineers, geologists, metallurgists, educators, students and researchers. SME advances the worldwide mining and underground construction community through information exchange and professional development.

ebook ISBN 978-0-87335-516-2